Novel Amioalkyl Tris-cyclometalated Iridium Complexes as Cellular Stains

A. Sansee, S. Meksawangwong, K Chainok, K.J. Franz, M. Gal, L.–O. Pålsson, W. Puniyan, R. Traiphol, R. Pal and F. Kielar

filipkielar@nu.ac.th

Department of Chemistry, Naresuan University, Phitsanulok, 65000, Thailand.
Department of Chemistry and Materials Technology, Thammasat University, Patum Thani, 12130, Thailand
Deparmtnet of Chemistry, Duke University, Durham, NC, 27708, USA
Department of Chemistry, Slovak Technical University, Bratislava, Slovakia
Deprtment of Chemistry, Durham University, Durham, DH1 3LE, UK
Laboratory of Advanced Polymers and Nanomaterials, Department of Chemistry and Center for Innovation in Chemistry, Naresuan University, Phitsanulok, 65000, Thailand
Program in Mateials Science, Mahidol University, Faculty of Science Bangkok, 10400, Thailand
NANOTEC-MU Excellence Center on Intelligent Materials and Systems, Mahidol University, Faculty of Science, Bangkok, 10400, Thailand
Center of Excellence in Biomaterials, Naresuan University, Phitsanulok, 65000, Thailand

Supporting Information

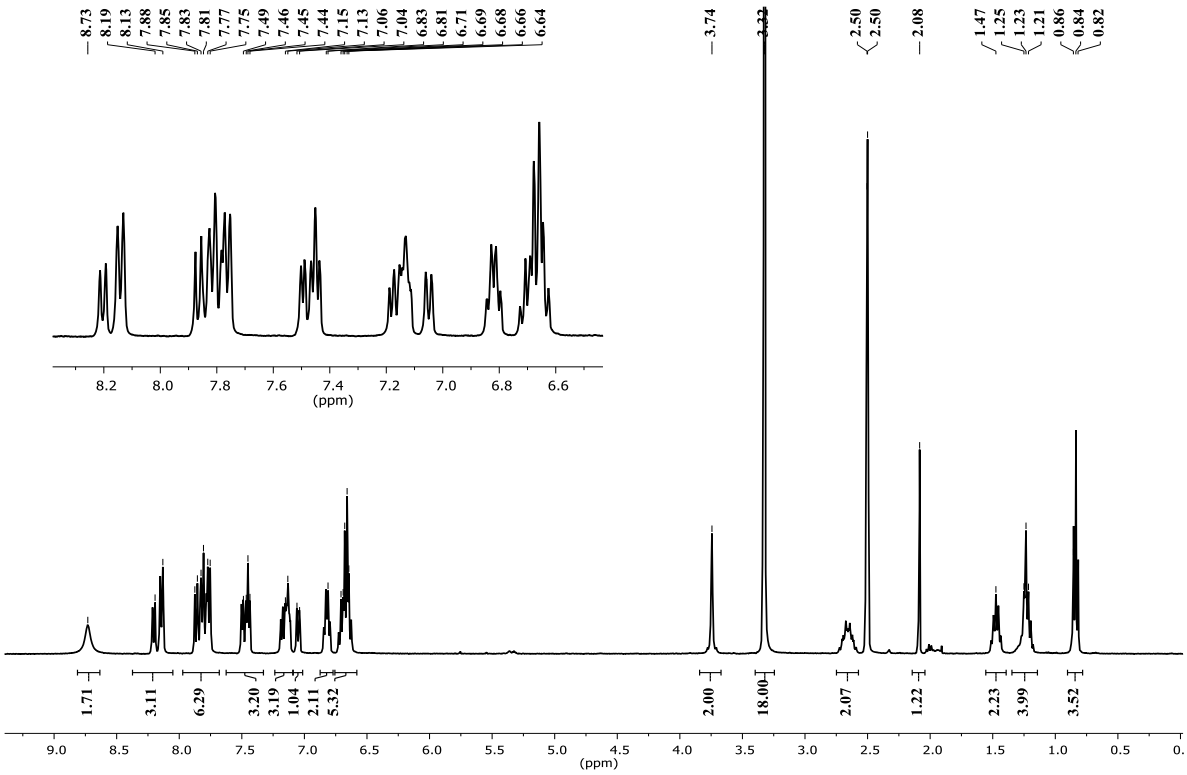

Figure S1 ^{1}H NMR spectrum of complex **1** in DMSO-d_6

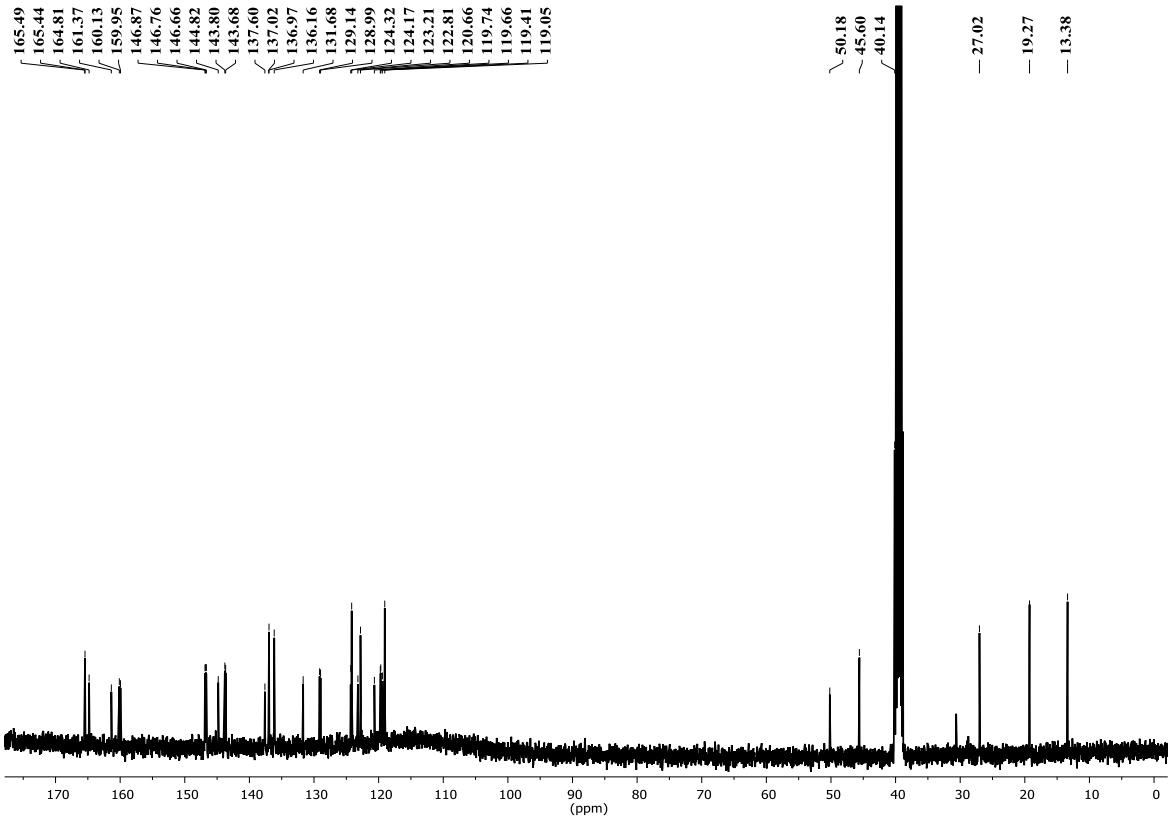

Figure S2 ^{13}C NMR spectrum of complex 1 in DMSO-d_6

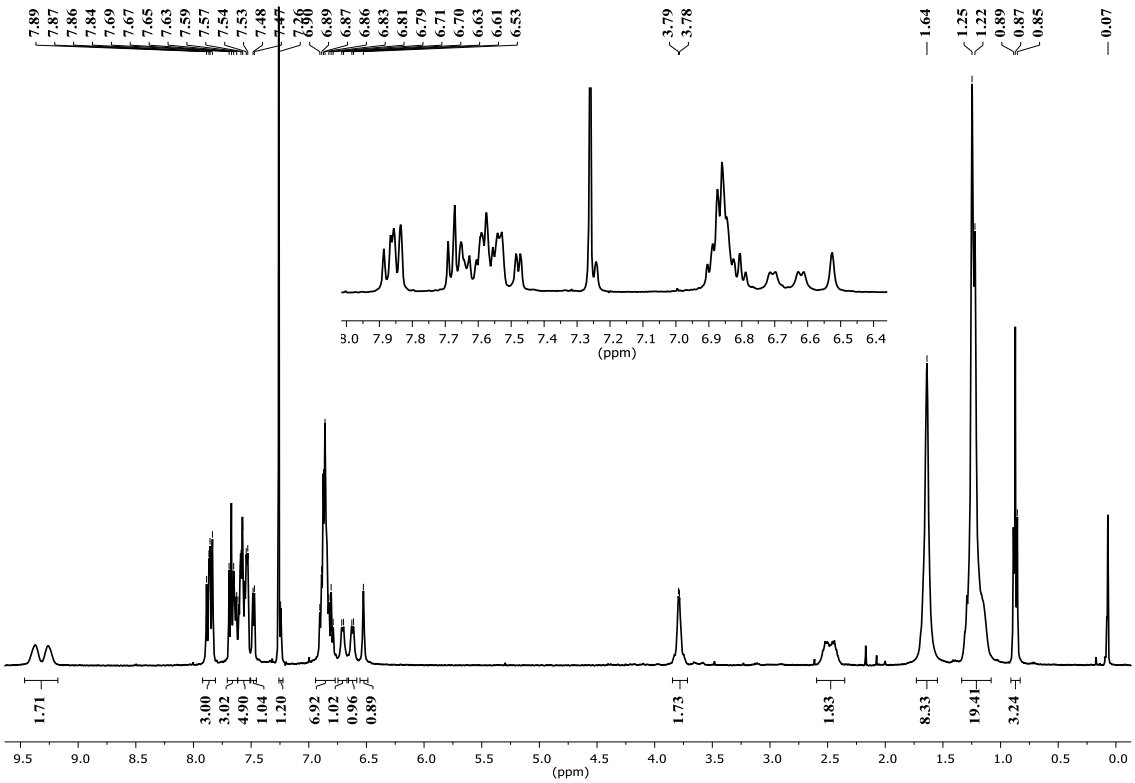

Figure S3 ^{1}H NMR spectrum of complex 2 in $CDCl_3$ (increased integral value for signal around 1.6 ppm is attributed to the presence of water)

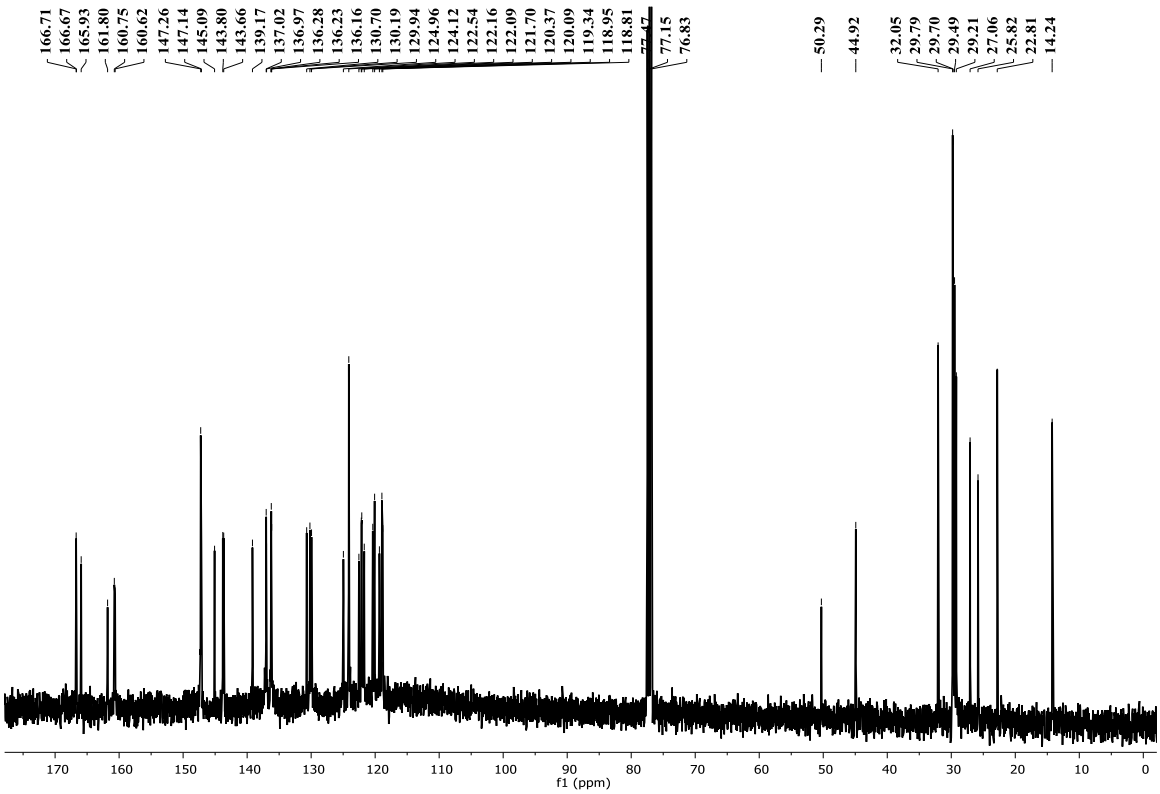

Figure S4 ^{13}C NMR spectrum of complex 2 in $CDCl_3$

Table S1 X-Ray data collection.

Crystal data	
Chemical formula	$C_{38}H_{36}IrN_4 \cdot Cl$
M_r	776.36
Crystal system, space group	Monoclinic, $P2_1/c$
Temperature (K)	296
a, b, c (Å)	11.8667 (10), 34.630 (3), 18.1372 (15)
β (°)	90.037 (2)
V (Å^3)	7453.3 (11)
Z	8
Radiation type	Mo $K\alpha$
μ (mm^{-1})	3.68
Crystal size (mm)	0.26 × 0.14 × 0.12
Data collection	
Diffractometer	Bruker D8 QUEST CMOS
Absorption correction	Multi-scan *SADABS2014*/4 (Bruker,2014/4) was used for absorption correction. wR_2(int) was 0.0857 before and 0.0616 after correction. The Ratio of minimum to maximum transmission is 0.8303. The λ/2 correction factor is 0.00150.
T_{min}, T_{max}	0.619, 0.745
No. of measured, independent and observed [$I > 2\sigma(I)$] reflections	144870, 14223, 10733
R_{int}	0.071
$(\sin \theta/\lambda)_{max}$ (Å^{-1})	0.613
Refinement	
$R[F^2 > 2\sigma(F^2)]$,$wR(F^2)$, S	0.037, 0.079, 1.04
No. of reflections	14223
No. of parameters	795
No. of restraints	21
H-atom treatment	H-atom parameters constrained
$\Delta\rho_{max}$, $\Delta\rho_{min}$ (e Å^{-3})	1.48, −1.07

Table S2 Structure quality indicators.

Structure Quality Indicators

Reflections:	d min (Mo) 0.82	I/σ 22.3	Rint 7.05%	complete 99%
Refinement:	Shift 0.002	Max Peak 1.5	Min Peak -1.1	GooF 1.040

Data Plots: Diffraction Data

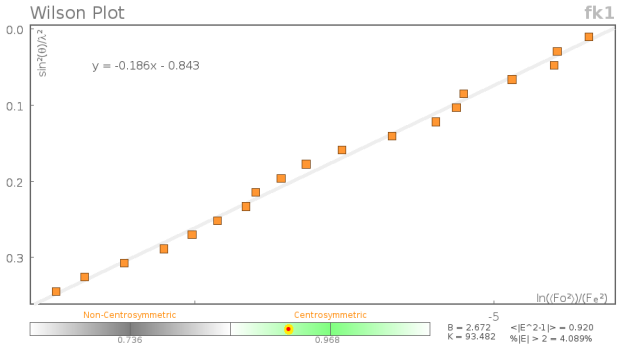

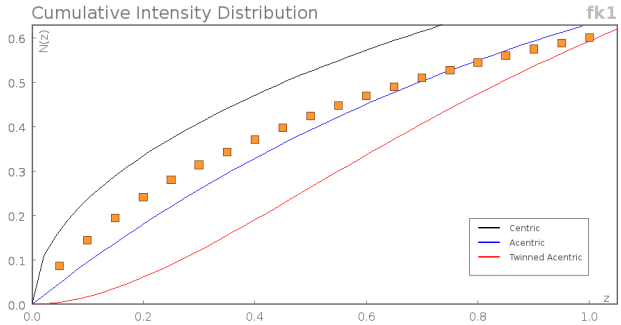

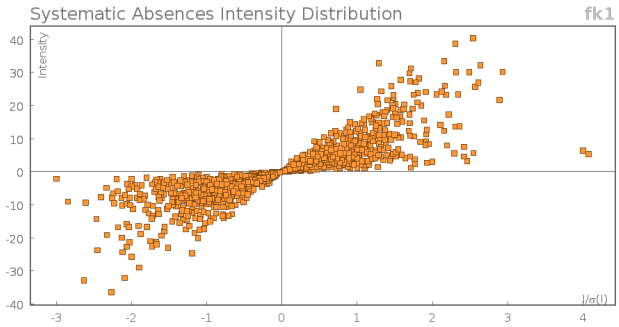

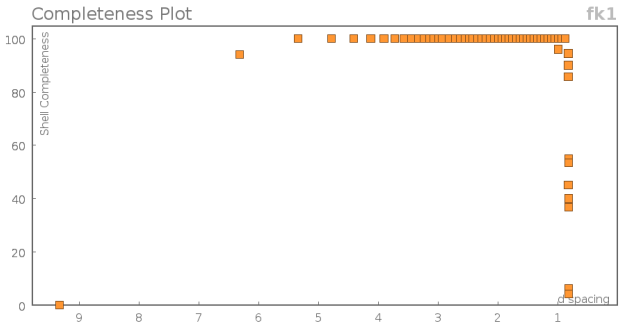

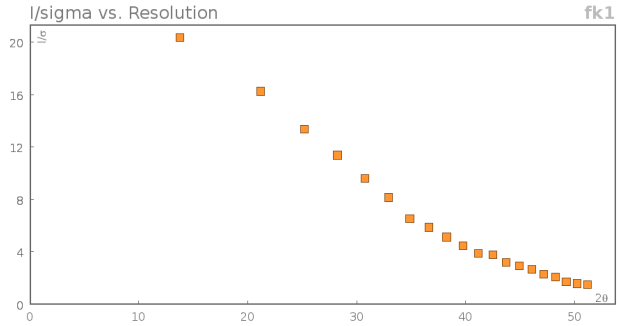

Data Plots: Refinement and Data

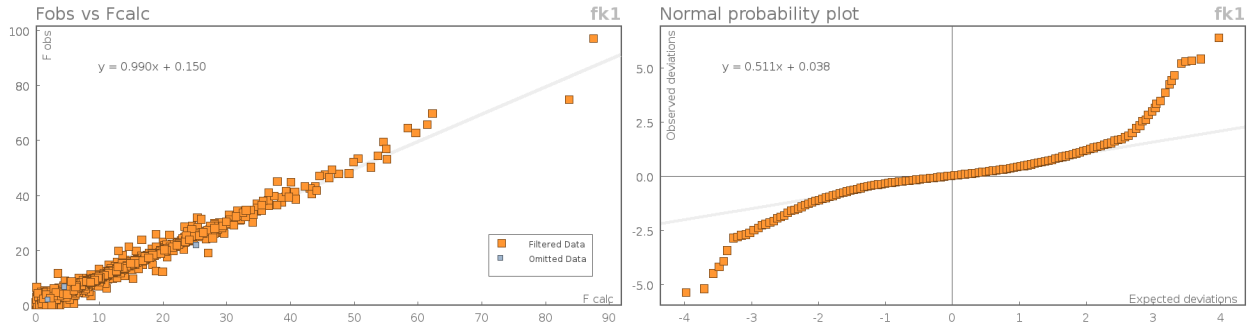

Figure S5 X-ray diffraction data.

Table S3 Reflection statistics.

Total reflections (after filtering)	144870	Unique reflections	14223
Completeness	0.991	Mean I/σ	22.3
hkl_{max} collected	(14, 42, 22)	hkl_{min} collected	(-14, -42, -22)
hkl_{max} used	(14, 42, 22)	hkl_{min} used	(-14, 0, 0)
Lim d_{max} collected	100.0	Lim d_{min} collected	0.36
d_{max} used	7.06	d_{min} used	0.82
Friedel pairs	24201	Friedel pairs merged	1
Inconsistent equivalents	0	R_{int}	0.0705
R_{sigma}	0.0432	Intensity transformed	0
Omitted reflections	0	Omitted by user (OMIT hkl)	30
Multiplicity	(9733, 12716, 13796, 13486, 2661, 178)	Maximum multiplicity	19
Removed systematic absences	1679	Filtered off (Shel/OMIT)	0

Table S4 Selected geometric parameters (Å, º).

Ir1−N1	2.123 (4)	Ir2−N5	2.134 (4)
Ir1−N2	2.129 (4)	Ir2−N6	2.108 (4)
Ir1−N3	2.119 (4)	Ir2−N7	2.136 (4)
Ir1−C11	2.003 (5)	Ir2−C49	2.011 (5)
Ir1−C22	2.016 (4)	Ir2−C60	2.014 (5)
Ir1−C33	2.010 (4)	Ir2−C71	2.019 (4)
N1−Ir1−N2	94.71 (14)	N5−Ir2−N7	94.02 (14)
N3−Ir1−N1	93.92 (15)	N6−Ir2−N5	93.77 (16)
N3−Ir1−N2	95.20 (15)	N6−Ir2−N7	93.55 (15)
C11−Ir1−N1	79.26 (17)	C49−Ir2−N5	78.87 (17)
C11−Ir1−N2	171.53 (16)	C49−Ir2−N6	171.40 (16)
C11−Ir1−N3	91.16 (16)	C49−Ir2−N7	91.43 (15)
C11−Ir1−C22	95.15 (18)	C49−Ir2−C60	95.86 (18)
C11−Ir1−C33	97.35 (18)	C49−Ir2−C71	95.80 (17)
C22−Ir1−N1	93.26 (15)	C60−Ir2−N5	89.17 (16)
C22−Ir1−N2	79.15 (17)	C60−Ir2−N6	79.44 (18)
C22−Ir1−N3	171.21 (16)	C60−Ir2−N7	172.49 (17)
C33−Ir1−N1	172.47 (16)	C60−Ir2−C71	98.13 (17)
C33−Ir1−N2	89.32 (16)	C71−Ir2−N5	171.42 (16)
C33−Ir1−N3	79.36 (17)	C71−Ir2−N6	92.02 (16)
C33−Ir1−C22	93.74 (17)	C71−Ir2−N7	79.28 (16)

Table S5 Hydrogen-bond geometry (Å, º)

D−H···*A*	*D*−H	H···*A*	*D*···*A*	*D*−H···*A*
N4−H4*A*···Cl1^{i}	0.89	2.26	3.112 (4)	161
N4−H4*B*···Cl2^{i}	0.89	2.19	3.077 (4)	174
C1−H1···N2	0.93	2.68	3.243 (6)	120
N8−H8*A*···Cl1	0.89	2.28	3.140 (4)	162
N8−H8*B*···Cl2	0.89	2.27	3.159 (4)	173

Symmetry code: (i) *x*+1, −*y*+1/2, *z*−1/2.

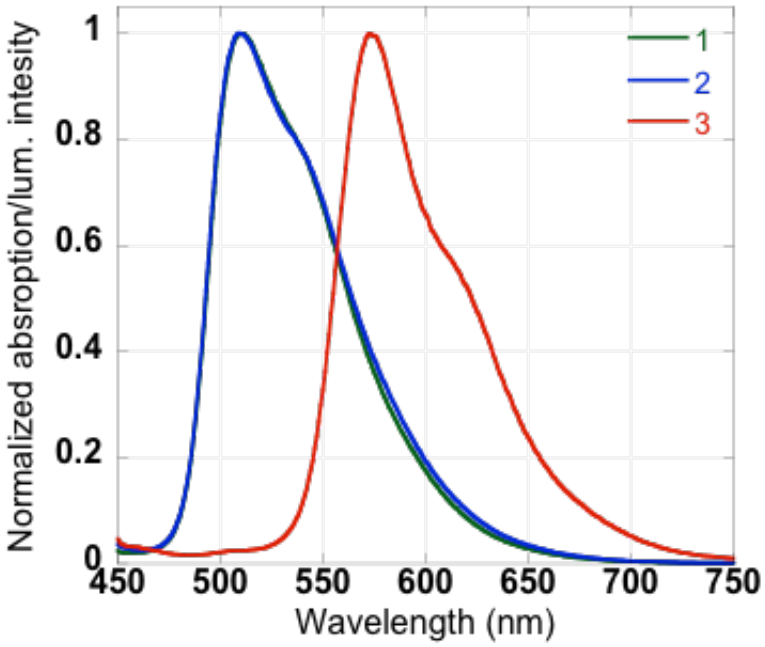

Figure S6 Normalized emission spectra of complexes **1** and **2** (10 μM) in toluene (λ_{ex} = 375 nm).

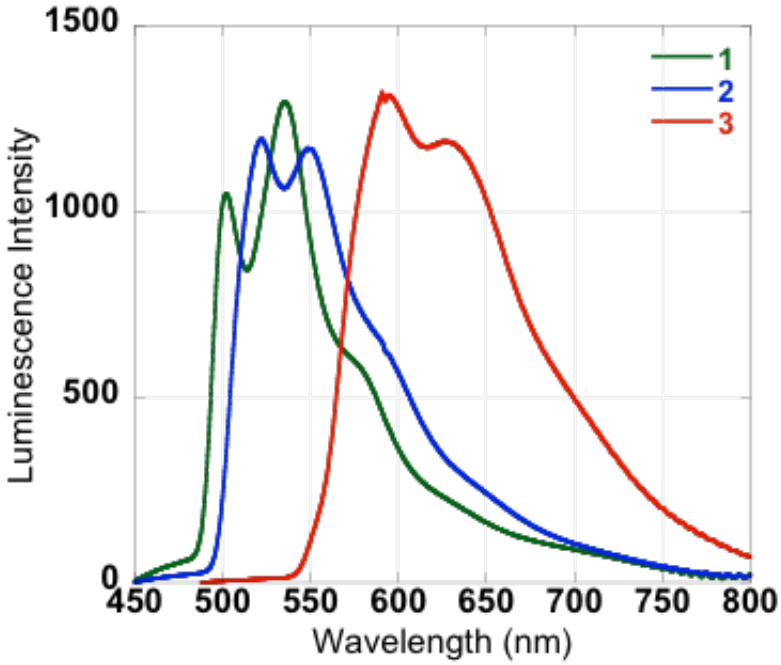

Figure S7 Low temperature emission spectra for iridium complexes **1**, **2**, and **3**.

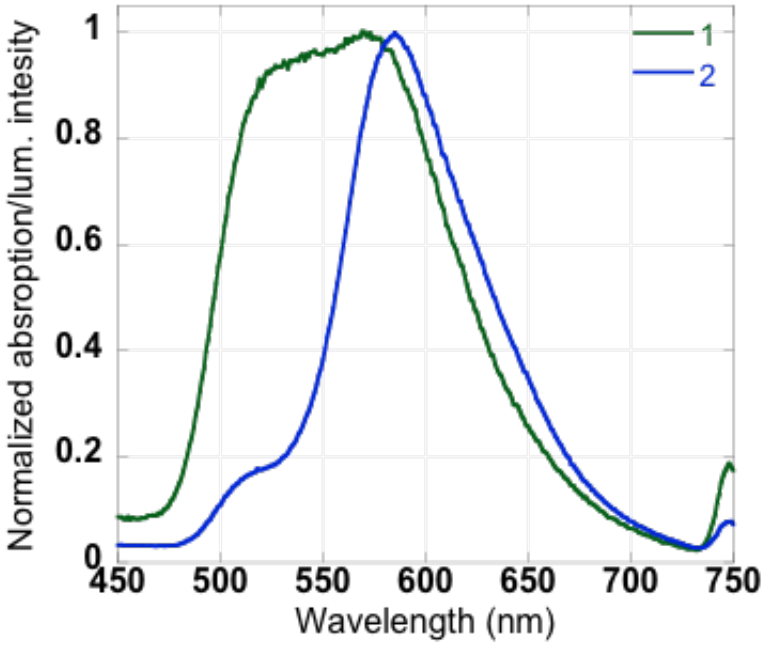

Figure S8 Normalized emission spectra of complexes **1** and **2** (1 μM) in phosphate buffer at pH 7.5 (λ_{ex} = 375 nm).

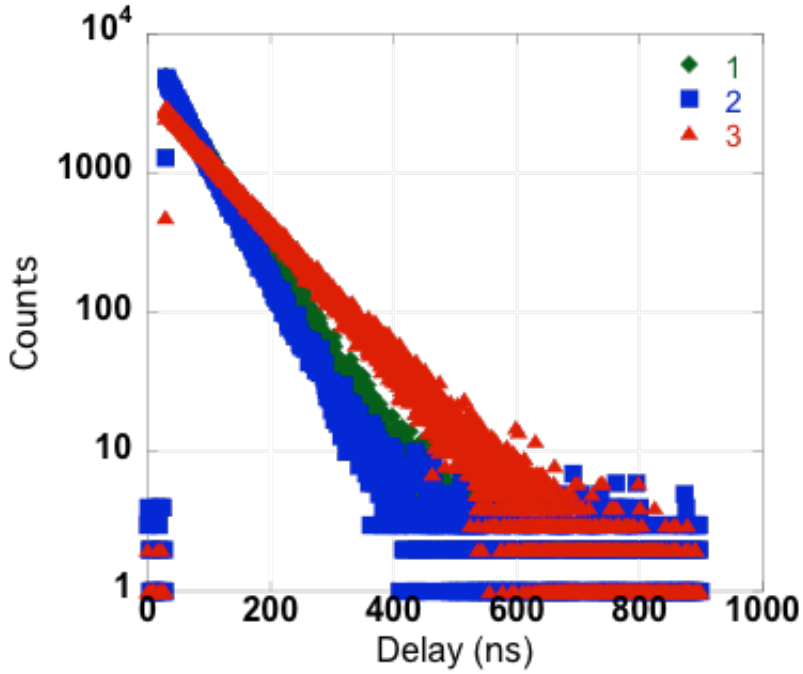

Figure S9 Emission intensity decays for complexes **1**, **2**, and **3** (10 μM) in air equilibrated DCM.

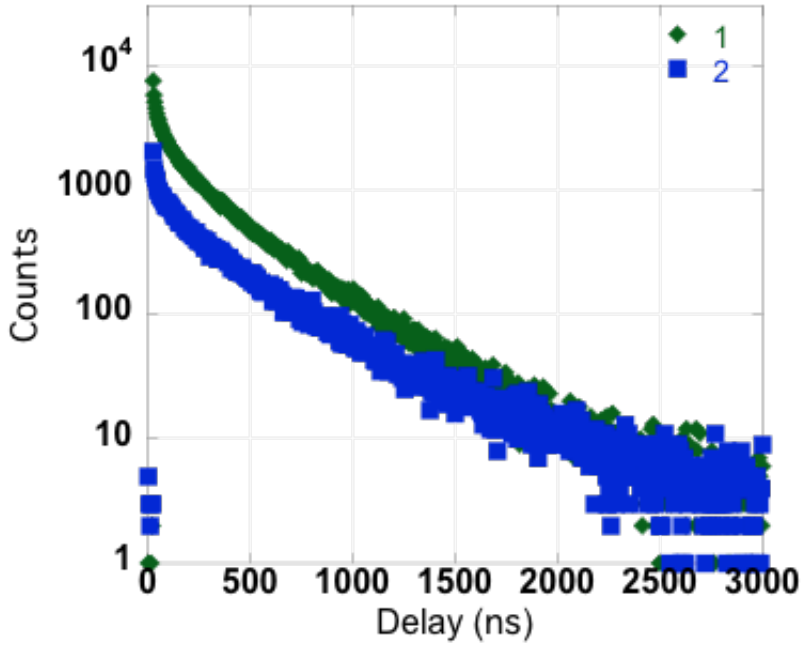

Figure S10. Emission intensity decays for complexes **1** and **2** (10 μM) in air equilibrated phosphate buffer (50 mM, pH 7.5).

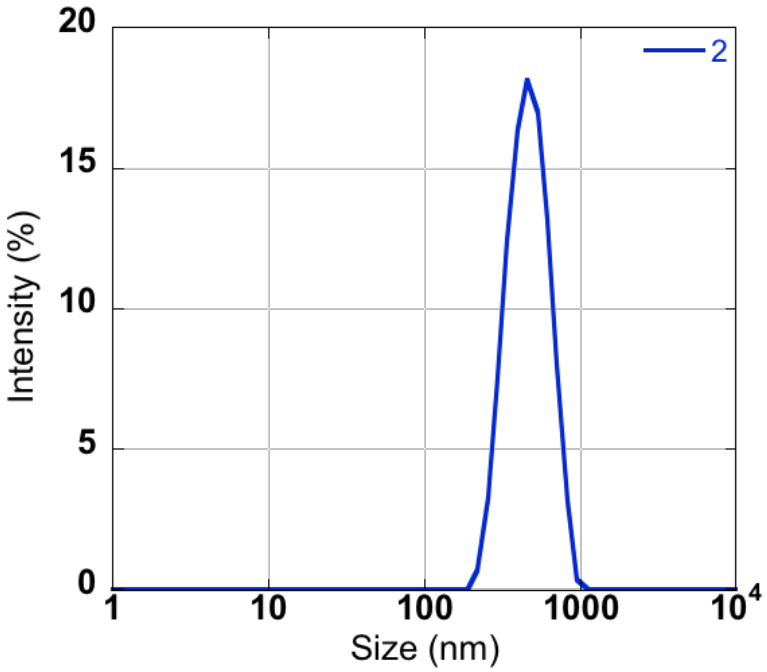

Figure S11 A dynamic light scattering plot for complex **2** in a mixture of water (60% v/v) and acetonitrile (40% v/v)

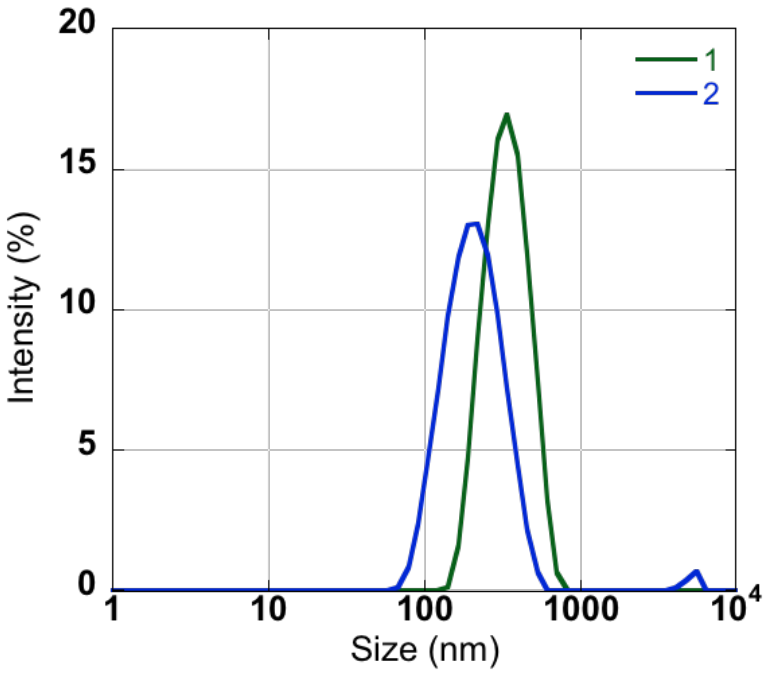

Figure S12 A dynamic light scattering plot for complexes **1** and **2** in a mixture of water (80% v/v) and acetonitrile (20% v/v)

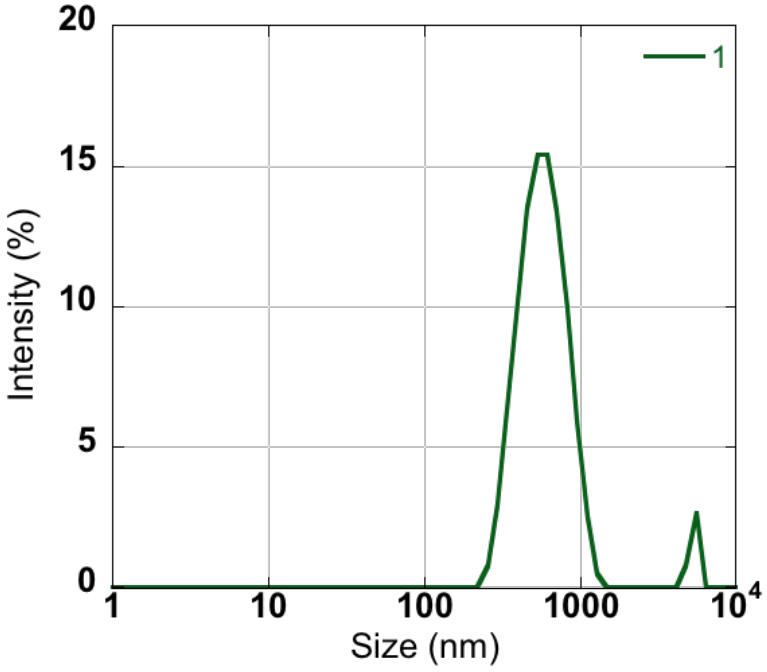

Figure S13 A dynamic light scattering plot for complex **1** in water

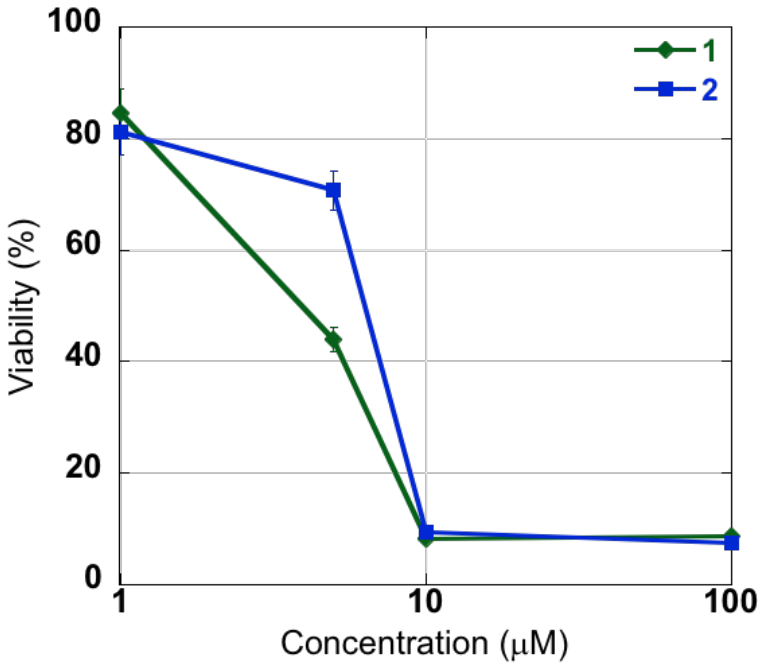

Figure S14 Viability of NIH-3T3 cells after 24 h exposure complexes **1** and **2**.

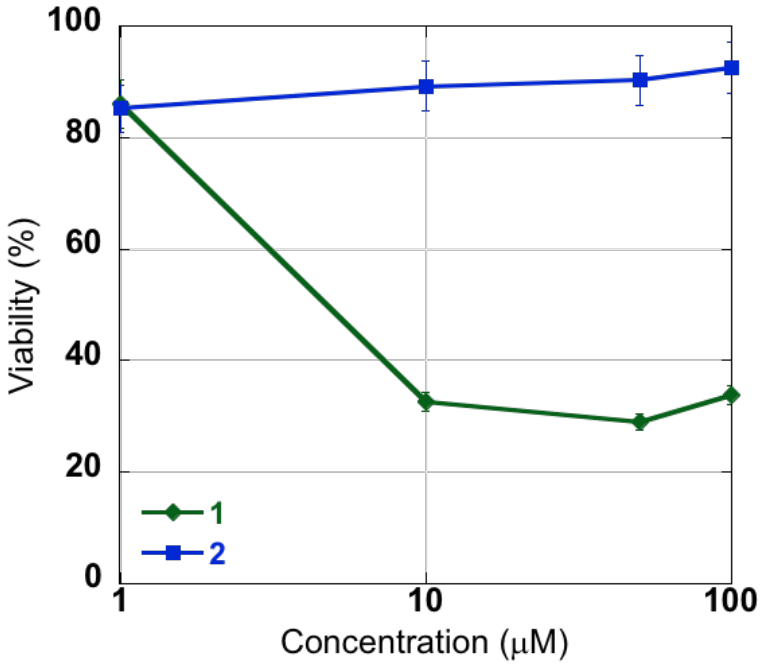

Figure S15 Viability of NIH-3T3 cells after 1 h exposure complexes **1** and **2**.

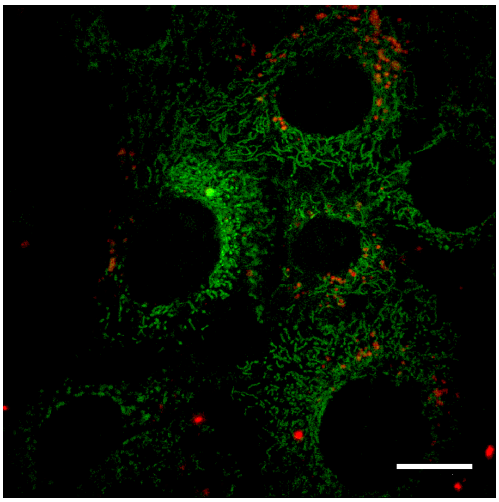

Figure S16 Fluorescence images obtained with complex **3** in NIH-3T3 cell (λ_{ex} 355 nm, λ_{em} 450-650nm). Complex **3** emission is located in the red spots. Green emission is autofluorescence of the mitochondria (λ_{ex} 355 nm, λ_{em} 400-450nm). (Scale bar: 10 μm)

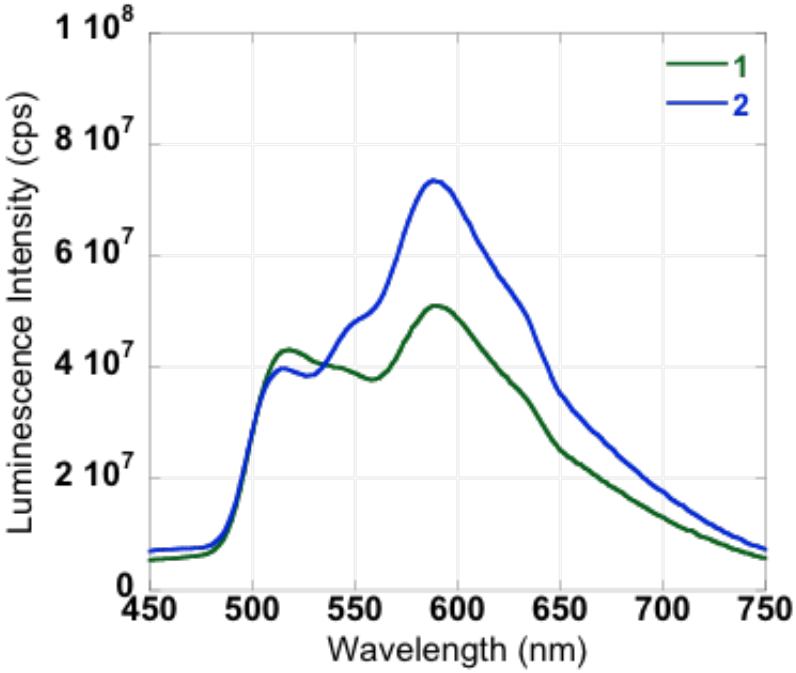

Figure S17 Emission spectra obtained from cell lysate of cells exposed to complexes **1** and **2**.

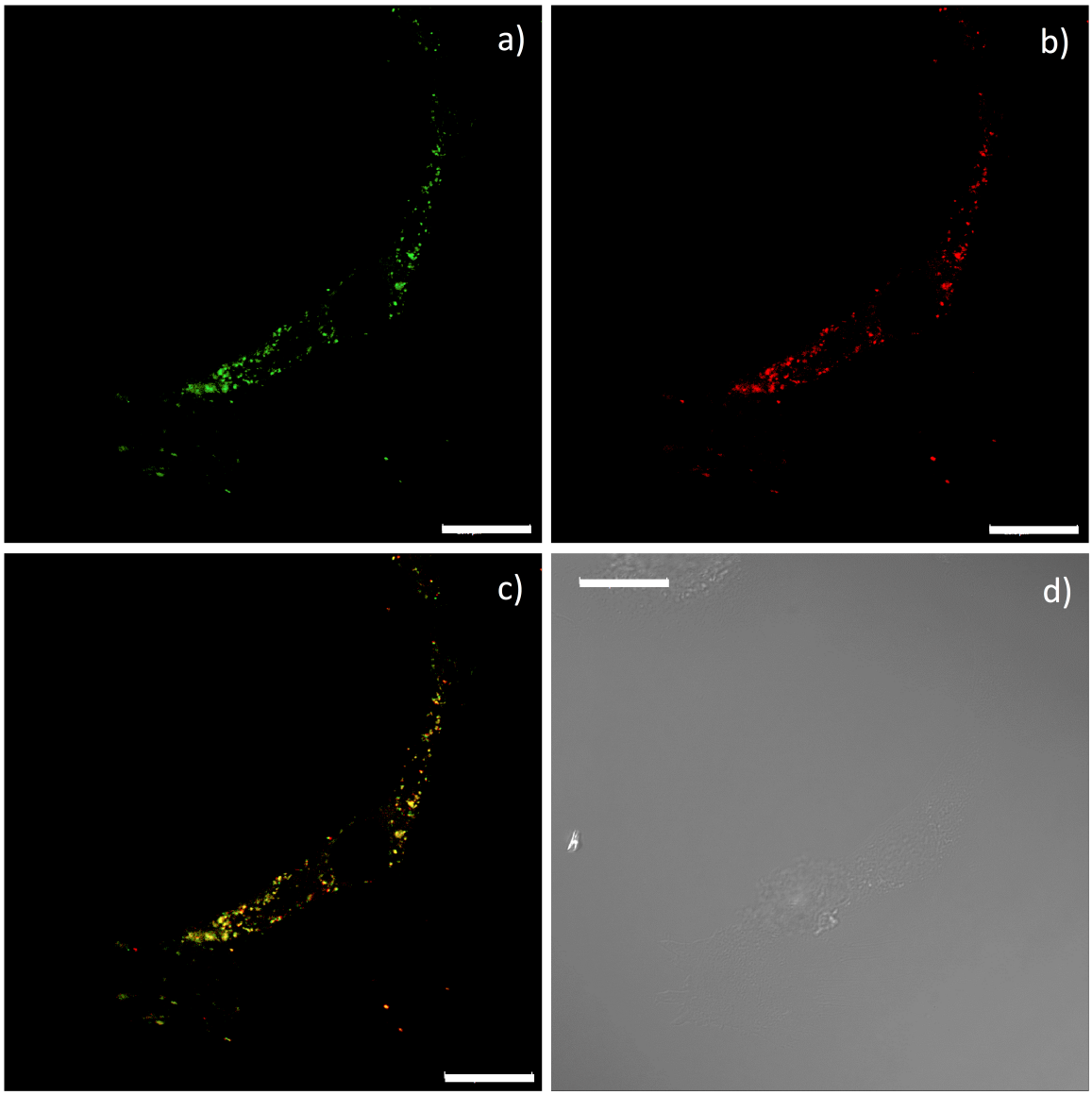

Figure S18 Fluorescence microscopy images obtained with complex **2** (1 μM loading for 1h) in NIH-3T3 cells after loading at 4°C. Panel a) shows emission of complex **2** (λ_{ex} 355 nm, λ_{em} 450-650nm), panel b) shows emission of lysotracker red stain (λ_{ex} 543 nm HeNe laser, λ_{em} 600-650 nm), panel c) shows an RGB overlay of the two fluorescence channels: P = 0.89, and panel d) shows the brighfield microscopy image. (Scale bar: 20 μm)

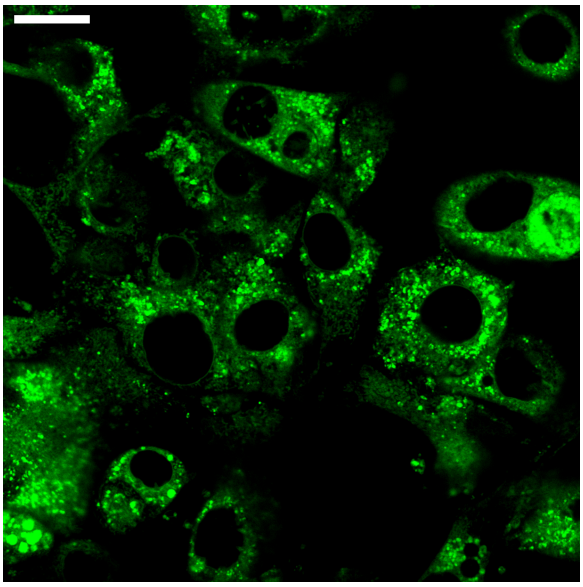

Figure S19 Confocal fluorescence microscopy image obtained with complex **2** using excitation at 405 nm. (λ_{em} 450-650nm). (Scale bar: 20 μm)

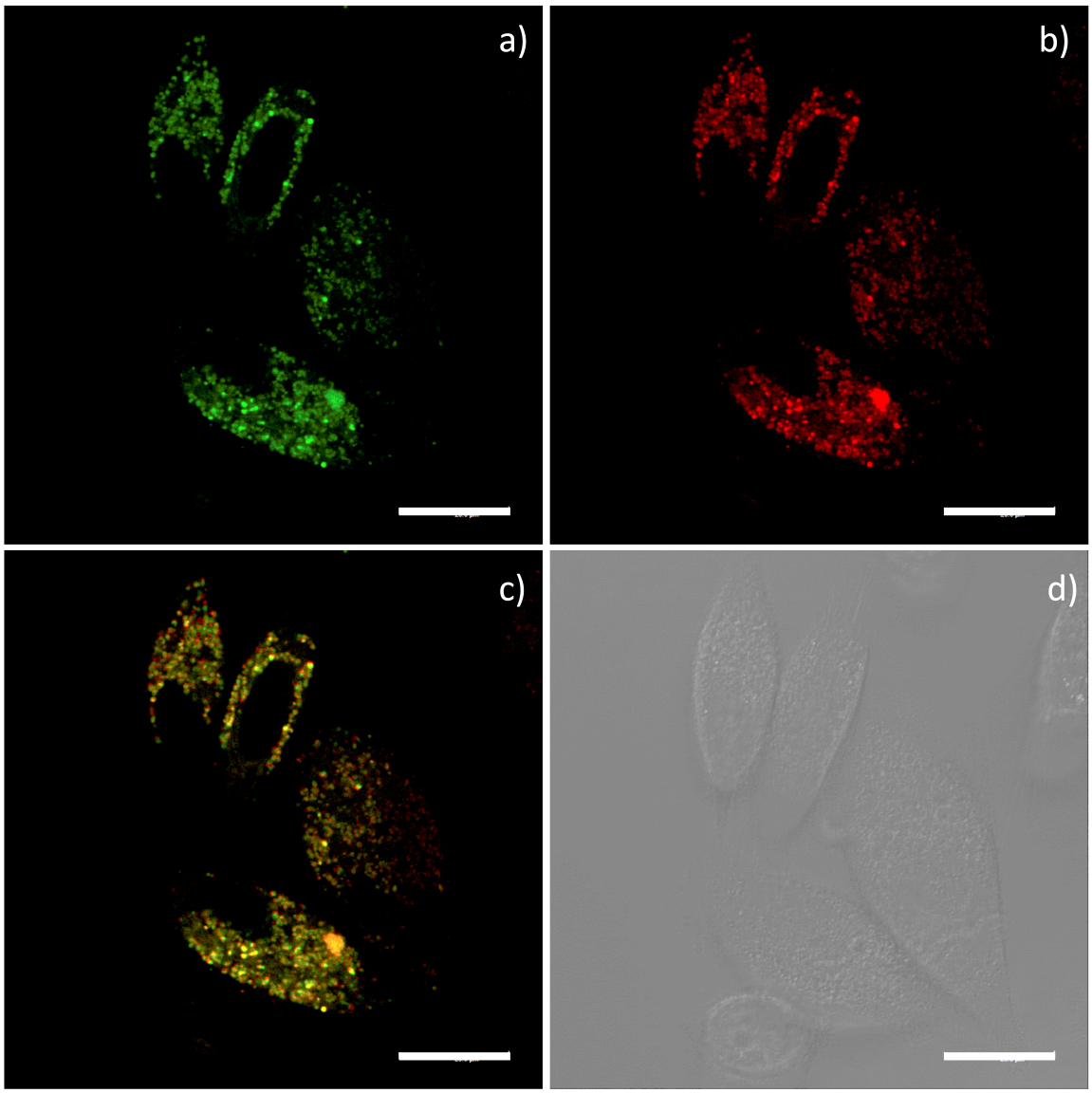

Figure S20 Fluorescence microscopy images obtained with complex **2** (1 μM loading for 1h) in PC3 cells. Panel a) shows emission of complex **2** (λ_{ex} 355 nm, λ_{em} 450-650nm), panel b) shows emission of lysotracker red stain (λ_{ex} 543 nm HeNe laser, λ_{em} 600-650 nm), panel c) shows an RGB overlay of the two fluorescence channels; P = 0.75, and panel d) shows the brighfield microscopy image. (Scale bar: 20 μm)

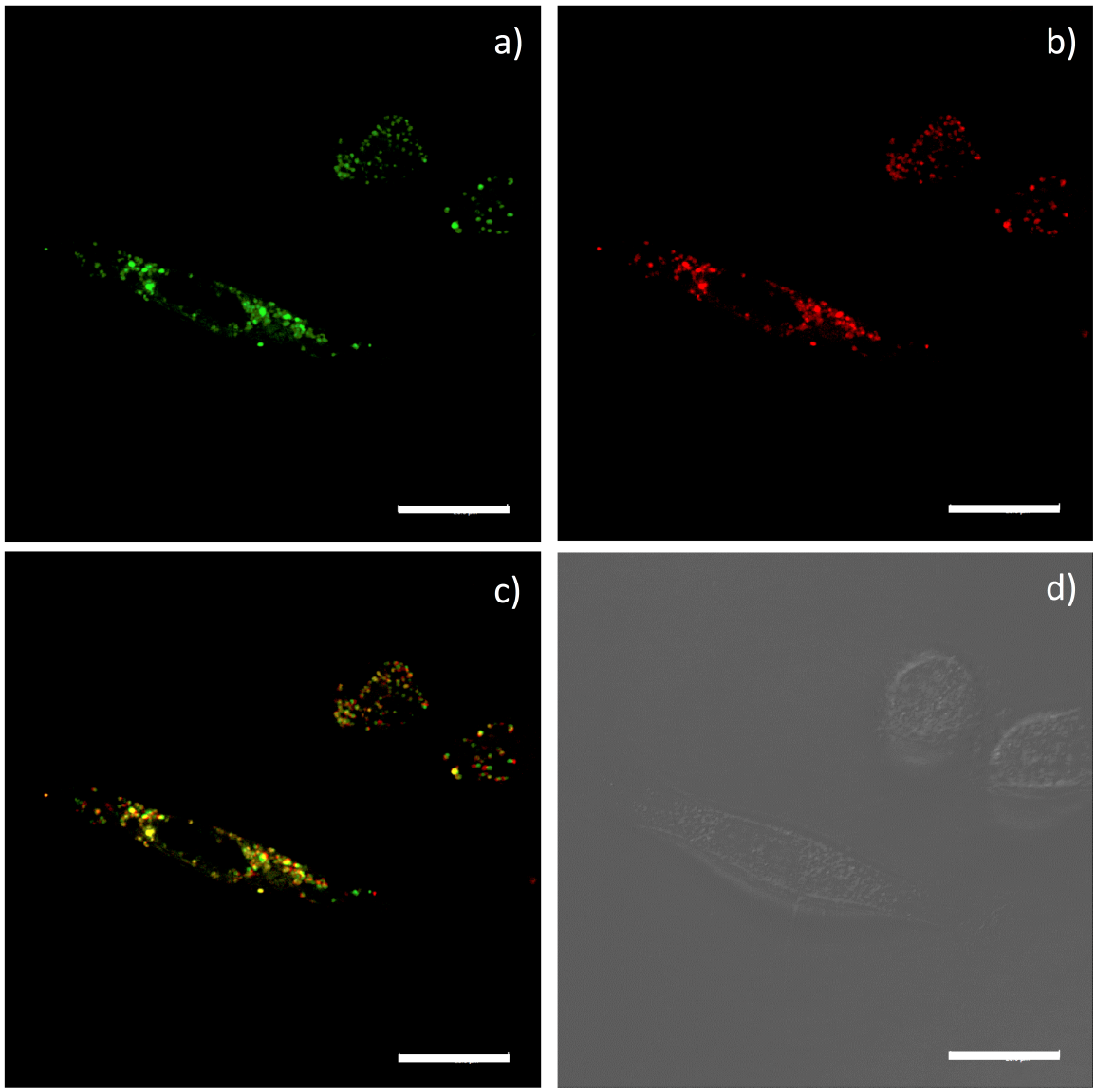

Figure S21 Fluorescence microscopy images obtained with complex **2** (1 μM loading for 1h) in NIH-3T3 cells after adjusting lysosomal pH to 5.5. Panel a) shows emission of complex **2** (λ_{ex} 355 nm, λ_{em} 450-650nm), panel b) shows emission of lysotracker red stain (λ_{ex} 543 nm HeNe laser, λ_{em} 600-650 nm), panel c) shows an RGB overlay of the two fluorescence channels P = 0.82, and panel d) shows the brighfield microscopy image. (Scale bar: 20 μm)

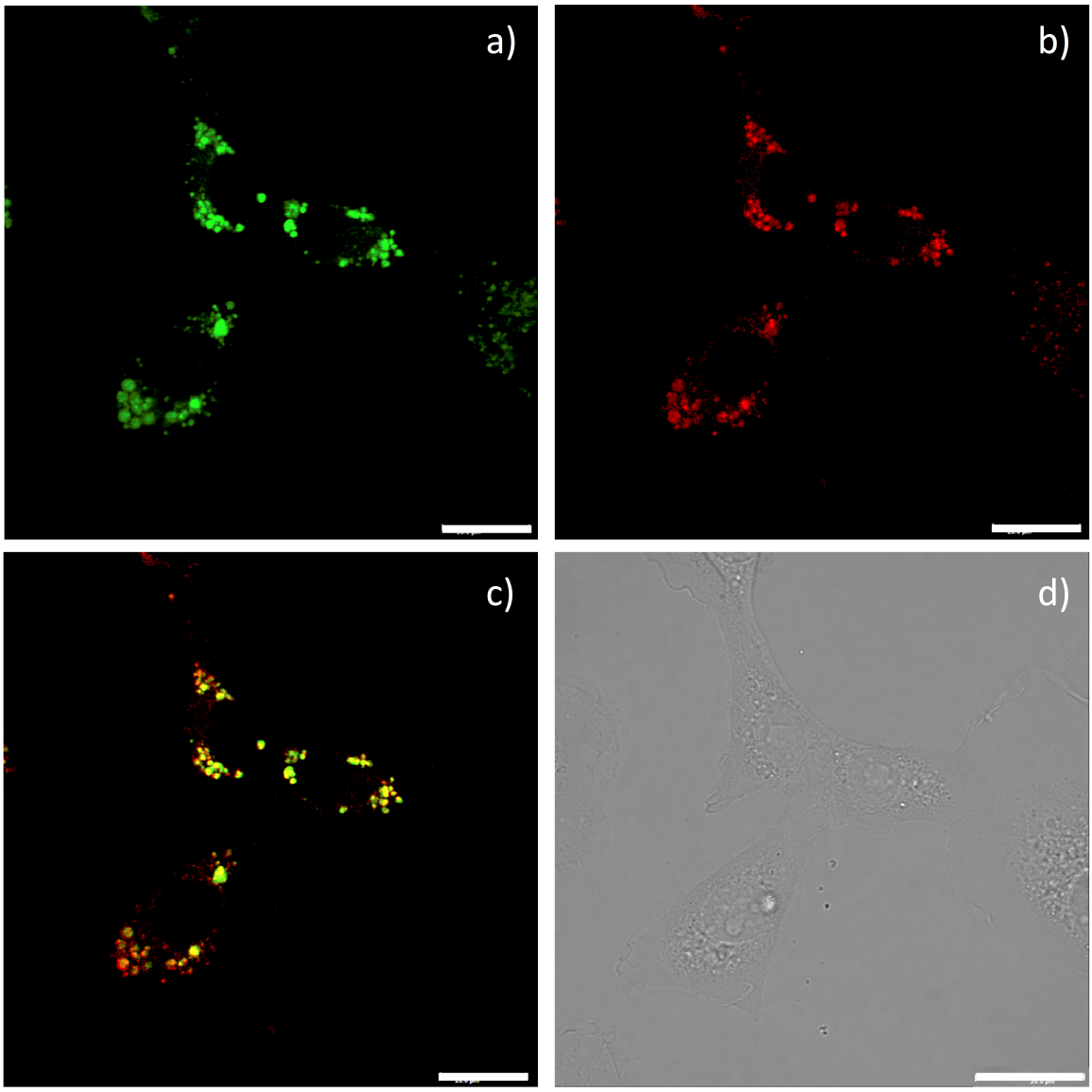

Figure S22 Fluorescence microscopy images obtained with complex **2** (1 μM loading for 1h) in NIH-3T3 cells after adjusting lysosomal pH to 6.6 using treatment of Chloroquine[1] 100 nM, 30 mins Panel a) shows emission of complex **2** (λ_{ex} 355 nm, λ_{em} 450-650nm), panel b) shows emission of lysotracker red stain (λ_{ex} 543 nm HeNe laser, λ_{em} 600-650 nm), panel c) shows an RGB overlay of the two fluorescence channels; P = 0.77, and panel d) shows the brighfield microscopy image. (Scale bar: 20 μm)

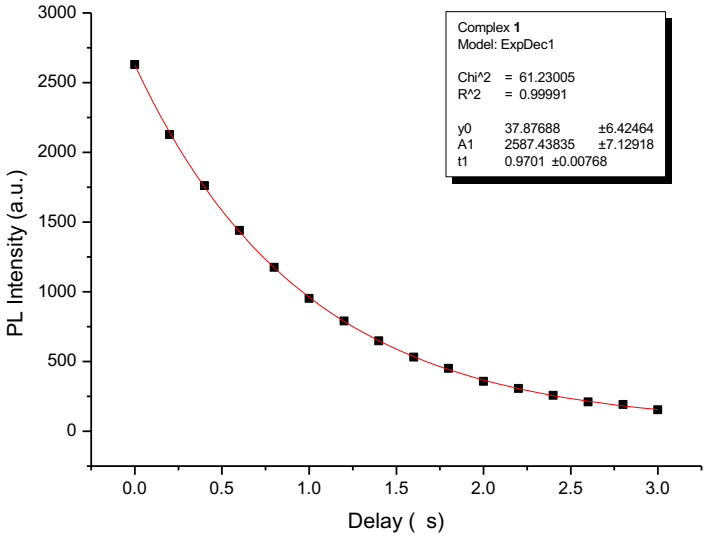

Figure S23 Emission intensity decay for complex **1** in NIH-3T3 cells.

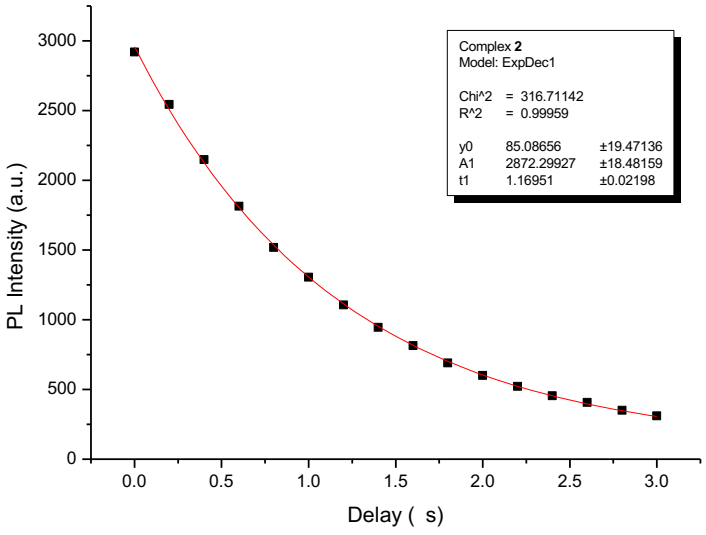

Figure S24 Emission intensity decay for complex **2** in NIH-3T3 cells.

1. D. G. Smith, B. K. McMahon, R. Pal and D. Parker, *Chem Commun (Camb)*, 2012, **48**, 8520-8522.